ADVANCED MATERIALS INTERFACES

www.advmatinterfaces.de

Clustering and Self-Recovery of Slanted Hydrogel Micropillars

Hyemin Lee, Jun-Hyun Kim, Gaoxiang Wu, Hae-Min Lee, Jaekyoung Kim, Dokyeong Kwon, Shu Yang, Chang-Koo Kim, and Hyunsik Yoon**

Slanted high-aspect-ratio polymer pillars are studied for their unique properties such as unidirectional spreading of liquid, directional adhesions, or alignment of cells, where the pillars are in constant contact with water or in a humid environment. These pillars, however, tend to cluster upon water evaporation due to the capillary force and lowered modulus of the pillars. Here, spontaneous recovery of clustered slanted hydrogel pillars to their original shape is presented by exploiting the modulus change of hydrogel materials during water evaporation. The clustering and recovery of the slanted hydrogel micropillars are monitored in situ by optical microscopy and environmental scanning electron microscopy. To elucidate sequential clustering and recovery mechanism, the adhesion force between the pillars and the restoring force is compared. Finally, the dynamic change of optical transparency is exploited as the result of switching between clustering and recovery of the slanted micropillars for display. The study of the deformation and recovery of slanted hydrogel pillars will offer insights into geometrical and material designs in water-based applications.

H. Lee, Prof. H. Yoon
Department of New Energy Engineering
Seoul National University of Science and Technology
Seoul 01811, Republic of Korea
E-mail: hsyoon@seoultech.ac.kr

J.-H. Kim, H.-M. Lee, Prof. C.-K. Kim
Department of Chemical Engineering and Department of Energy Systems Research
Ajou University
Suwon 16499, Republic of Korea
E-mail: changkoo@ajou.ac.kr

G. Wu, Prof. S. Yang
Department of Materials Science and Engineering
University of Pennsylvania
3232 Walnut Street, Philadelphia, PA 19104-6272, USA

J. Kim, Prof. H. Yoon
Department of Chemical and Biomolecular Engineering
Seoul National University of Science and Technology
Seoul 01811, Republic of Korea

Dr. D. Kwon
The National Creative Research Initiative Center for Intelligent Hybrids
Seoul National University
Seoul 08826, Republic of Korea

The ORCID identification number(s) for the author(s) of this article can be found under https://doi.org/10.1002/admi.201801142.

DOI: 10.1002/admi.201801142

High-aspect-ratio (HAR) micro- and nanopillars are of great interests for potential applications, including gecko-inspired dry adhesives,[1,2] superhydrophobic surfaces,[3] and tissue scaffolds to guide stem cell differentiation.[4] They are prepared by methods such as seeded growth of carbon nanotubes, deep etching of silicon, and replica molding of polymers.[5–7] Among them, polymers are most attractive because of their processability and low cost. However, HAR polymeric pillars tend to be clustered after exposure to water or humidity, which is common in ambient conditions and in many uses, due to capillary force during water evaporation.[8,9] Researchers have attempted to avoid the clustering by enhancing the modulus of the polymers[10] or coat a thin film of high-modulus inorganic materials (e.g., metal or silica) on the pillar surfaces.[11] Among various HAR pillars, slanted pillars offer directionality and have been utilized for selective adhesion, directed wetting, and preferential cell differentiation.[12,13] The directional properties generated by the asymmetric features of the pillars can be further exploited by the change of pillar tilting directions.[14] However, the HAR slanted pillars can also be clustered after experiments in water,[15] and cannot be reused again. Recently, we and others have reported to recover the clustered pillars using external forces such as ultrasonication or mechanical pulling to separate the adhered pillars.[16,17] However, the added extra processes could be inconvenient for some applications, and the uniformity of recovery is subject to the uniformity of the applied load. Here, we demonstrate spontaneous recovery of the clustered pillars to the original shape by taking the advantage of the change of elastic modulus of the hydrogels during swelling and drying processes. Hydrogel patterns have received intensive attention because of potential applications in smart bioanalytical systems. They can be utilized as smart valves in microfluidic devices or as actuating crease for stimuli-responsive drug delivery system.[18] In this work, we prepared the hydrogel HAR micropillars from poly(ethylene glycol diacrylate) (PEGDA) prepolymer mixed with a photoinitiator. We then monitored the clustering and recovering events in situ under an optical microscope and an environmental scanning electron microscope (ESEM). To understand the shape recovery, we compared the adhesion forces between pillars and the restoring forces from the clustered states. As

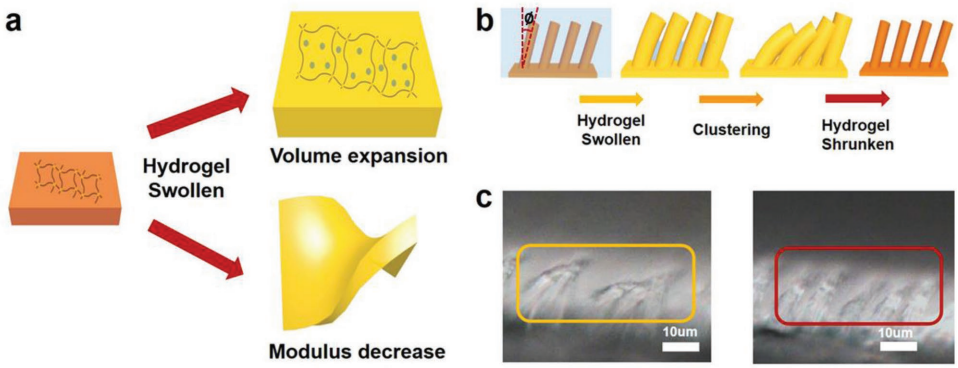

Figure 1. a) A schematic illustration of the swollen hydrogels with volume expansion or modulus change. b) Illustration of the clustering of slanted hydrogel micropillars and their recovery after drying. c) Cross-sectional optical microscopic images of the clustered micropillars (left) and recovered pillars (right).

a result of clustering and recovery of the slanted pillars, we exploited switching of optical transparency for display.

Figure 1a illustrates the concept of modulus and volume change of a hydrogel. Hydrogels are lightly cross-linked hydrophilic polymers and can absorb a large amount of water.[18] When water penetrates into the hydrogel network, the hydrogels undergo volumetric expansion and decrease of modulus where water acts as a plasticizer. Therefore, the pillars are clustered during initial evaporation of the water (Figure 1b). After drying of the hydrogel network, however, the hydrogel pillars are recovered to their original shape due to shrinkage in pillar size and increased elastic modulus. One of the examples is contact lenses. Soft contact lenses are typically made of silicone or silicone/hydrogels. They are rubbery in water and, thus, more comfortable to wear. However, if they are left in air for a long period of time, the lenses become brittle due to increased glass transition temperature (T_g) and modulus; they are in the glassy state and can be easily distorted. Here, we exploit the characteristic of hydrogels, which change modulus after swelling and drying from water. We have fabricated slanted hydrogel micropillars from PEGDA mixed with a photoinitiator by micromolding and investigated the clustering and shape recovery behaviors of slanted pillars. For our experiments, we prepared a silicon master fabricated by conventional photolithography, followed by the slanted etching process. The angles of sample holders are kept at 30° with respect to an electrode within a Faraday cage for the slanted etching. Then, we replica molded a polydimethylsiloxane (PDMS) mold from the Si master with a square array of pillars. To fabricate the slanted hydrogel pillars, we infiltrated the UV-curable PEGDA mixture into the PDMS mold, followed by UV curing (see details in the "Experimental Section" and in Figures S1 and S2 in the Supporting Information). Figure 1c shows the cross-sectional optical images of clustered and the recovered slanted micropillars, respectively. After directional clustering of the slanted pillars during initial water evaporation stage, interestingly, the pillars are recovered to the original shape after about drying for 1–2 min (see Movie S1 in the Supporting Information on changed states).

To better understand the clustering and shape recovery processes of the hydrogel pillars, we image the pillars in situ usingESEM (see **Figure 2**) and an optical microscope (see **Figure 3**). In ESEM, the temperature of the substrate and humidity within the chamber can be controlled during observation of the microstructures. Figure 2 shows schematic illustration and the corresponding ESEM images during clustering and recovery of the pillars (pillar diameter = 4 μm; spacing and height = 18 μm). After decreasing the substrate temperature and increasing humidity, we immerse the pillars in water as shown in Figure 2a. As the pillars begin to swell, their volume expands, and the modulus is decreased. Then, we increase the substrate temperature while decreasing humidity to evaporate off water outside and in-between the pillars. Figure 2b clearly shows that capillary force first induces the clustering of micropillars during evaporation of water in-between pillars. Then water absorbed within the hydrogel network starts to dry. The

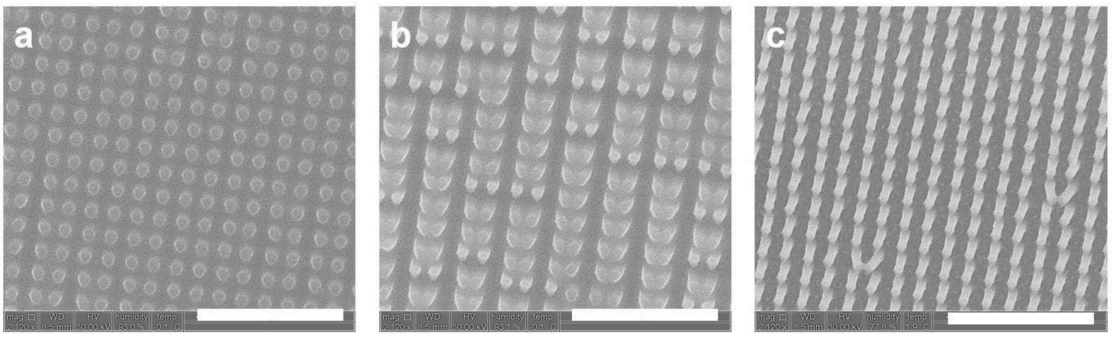

Figure 2. Environmental scanning electron microscopic (ESEM) images of slanted pillars a) immersed in water, b) clustered during water evaporation, and c) recovered after drying under vacuum (≈ 3 Torr). The scale bars are 50 μm.

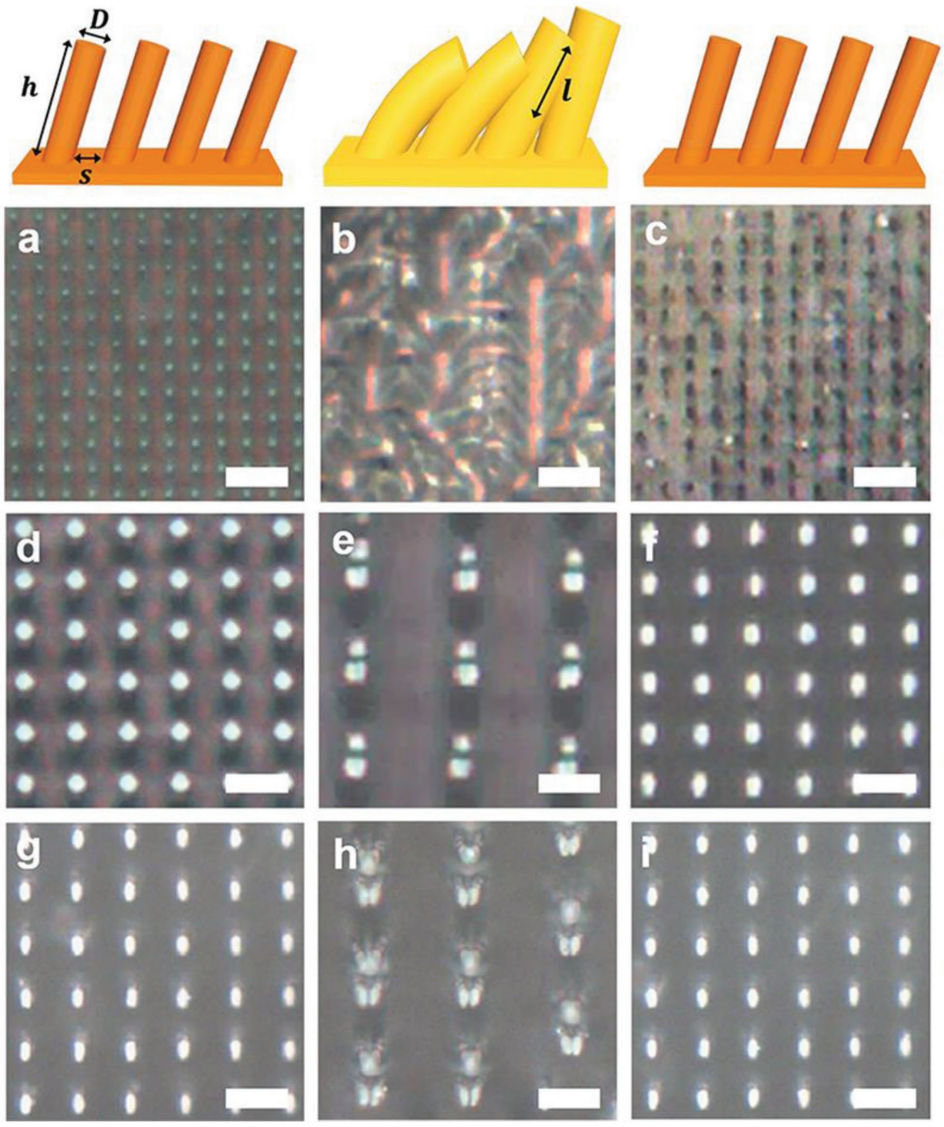

Figure 3. Optical microscopic images of the slanted pillars before (left panel) and after (middle panel) swelling and drying (right panel). The pillars are slanted by 30° from the straight one. a) Before swelling (diameter = 2 μm, height = 12 μm, and spacing = 2 μm); b) after swelling and clustering (diameter ≈ 2.4 μm, height ≈ 14.4 μm, and space ≈ 1.6 μm); and c) after water drying for 1 min. d) Before swelling (diameter = 4 μm, height = 12 μm, and spacing = 4 μm); e) after swelling and clustering (diameter ≈ 4.8 μm, height ≈ 14.4 μm, and spacing ≈ 3.2 μm); and f) after water evaporation for 75 s. g) Before swelling (diameter = 3 μm, height = 20 μm, and spacing = 5 μm); h) after swelling and clustering (diameter ≈ 3.6 μm, height ≈ 24 μm, and spacing ≈ 4.4 μm); and i) after water evaporation for 80 s. All scale bars are 10 μm.

loss of water inside of network leads to an increase in T_g of the hydrogel, and thus, Young's modulus.[19] As seen in Figure 2c, the pillars start to return to their original shape and are eventually recovered completely after dried.

In Figure 3, we show the slanted hydrogel pillars of different sizes before (left panels) and after (middle panels) swelling, and after drying (right panels), including pillars with the diameter and spacing of 2 μm and the height of 12 μm (aspect ratio, AR = H/D = 6) (Figure 3a–c); diameter and spacing of 4 μm and a height of 12 μm (AR = 3) (see Figure 3d–f); and pillars with 3 μm in diameter, 5 μm in spacing, and 20 μm in height (AR = 6.8) (see Figure 3g–i). All showed similar clustering and recovery behaviors. The reversible clustering–recovery behavior is confirmed by 20 cycles of repetition (see Figure S3 in the Supporting Information). We note the fabricated pillar diameters are slightly smaller than the original designs because of etching of the sidewall within the plasma system.

To analyze the origin of clustering and self-recovery phenomena, we examine the forces applied to the pillars during clustering and recovery. At first, capillary force during water evaporation (F_c) is the main driving force for clustering pillars, which is given by[10,15]

$$F_c = \frac{\pi\gamma D^2\cos^2\theta}{2\sqrt{(D+\delta)^2 - D^2}} \quad (1)$$

where γ is the surface tension of water (0.073 N m^{-1}), θ is the contact angle between water and pillar surface, and δ is the distance between the pillars after clustering by the capillary force. To cluster micropillars, the capillary force should be greater than the restoring force (F_{res}), which is elastic term to the original state[15]

$$F_{res} = \frac{3\pi EDS}{64(AR)^3} \quad (2)$$

where E is the Young's modulus of pillars. After pillars are clustered by capillary force, we should consider adhesion force (F_{ad}) between pillars, which can be derived as[20]

$$F_{adh} = \frac{A\sqrt{Dl}}{16\sqrt{2}D_c^{2.5}} \quad (3)$$

where l is the length of pillars when they overlap (≈10% of pillar height (H)), A is the Hamaker constant (6.4×10^{-20}J), and D_c is the cutoff length of the adjacent clustered pillars. By calculating the ratio of the restoring force versus the adhesion force (F_{res}/F_{adh}), we can estimate the pillar states, whether recovered and remained to be clustered.

Here, the change of modulus during drying from rubbery to glassy state along with increase of T_g of the hydrogel networks is critical to the magnitude of F_{res} and F_{adh}, and thus their ratios in the swollen and drying state. Meanwhile, the pillar volume also changes. To estimate how much volume increases when the hydrogel is fully swollen, we made a hydrogel cube that was left in water overnight to reach equilibrium. After fully swollen, the width and depth of the hydrogel cube were found to be increased by 18%, respectively, and the height was increased by 20%. Thereby, when the hydrogel pillars (cylindrical in shape) are fully swollen, the diameter is changed to 1.2D (=D_s), height is 1.2H (=H_s), and space is 0.8S (=S_s). We then calculated the restoring and adhesion forces using these values (D_s, H_s, S_s). Young's modulus of hydrogels is measured by an atomic force microscopy (AFM) as E = 54.84 ± 22.41 MPa (in the swollen state) and E = 199.7 ± 63.3 MPa (in the dry state) (see Figure S4 in the Supporting Information).

As seen in **Figure 4**, when pillars are short (original AR < 3 and swollen AR < 3.05), hydrogel pillars are not clustered upon swelling. In this case, the capillary force is not enough to overcome the elastic restoring force. When the aspect ratio increases to higher than 6, F_{res}/F_{adh} becomes smaller than unity and the pillars are clustered and cannot be recovered. At AR = 3–6, when water in the network of hydrogel evaporates, the F_{res}/F_{adh} ratio becomes larger than unity as the size of the pillar shrinks and modulus increases. Also, when we use slanted pillars, the spacing (S) between pillars is reduced to $S\cos\phi$, where ϕ is the tilting angle (here, 30°). In this regard, pillar H is increased to $H/\cos\phi$ because we use the same thickness of SiO_2 layers when we fabricate a master from slanted plasma etching. As shown in Figure 4, the pillars are clustered in the range of AR = 3–6 and they can be recovered to the original state by the increase of modulus.

Optical images are shown in **Figure 5**, further detailing the sequential clustering and recovery steps of the slanted pillars. As shown in Figure 5a, two pillars in the lateral direction (see yellow arrows in the inset) are clustered first, and then the slanted pillars are clustered together. It can be explained by the Kelvin equation which implies the low vapor pressure of a liquid in a porous media[21]

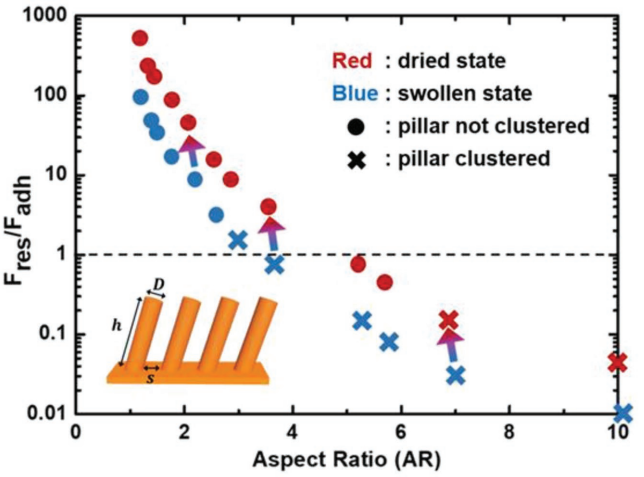

Figure 4. Ratio of the restoring force to the adhering force versus the aspect ratio (AR) of the slanted hydrogel pillars. In the high-AR region, pillars are clustered and not recovered (blue and red X). In the low-AR region, pillars are not clustered. At AR = 5, the clustered pillars are recovered after drying.

$$\ln\left(\frac{p}{p_0}\right) \sim -\frac{\nu_m \gamma}{SRT} \quad (4)$$

Here, p is the vapor pressure on the liquid meniscus between pillars, p_0 is the saturated vapor pressure, ν_m is the molar volume of a liquid, R is the gas constant, T is the absolute temperature, and γ is the surface tension of a liquid. The reduced distance between pillars ($S\cos\phi$) in a slanted direction (red arrows) results in the lower vapor pressure of water, leading to sequential clustering by late evaporation. After about 1–2 min, pillars started to recover in the lateral direction because the displacement between pillars in the lateral direction (indicated by the yellow arrows) is greater than that in the slanted direction due to stronger restoring force as shown in Equation (2). Finally, the pillars are recovered in the slanted direction.

Last, we exploit the visual effects of the slanted pillars during clustering and recovery. We placed the slanted pillars on the letters "SEOUL TECH." When the pillars are tilted, the hydrogel film is not transparent because of light scattering from the pillar surface (see **Figure 6**a). When the film is dipped in a water bath for 30 min, the film becomes transparent (Figure 6b) even after drying water by air blowing. When water trapped in the internal structures of hydrogel pillars begins to evaporate, the film becomes opaque because the pillars return to the slanted states (Figure 6c). To confirm the visual difference, we perform the optical simulation by commercial ray tracing software (LightTools). The pillars are slanted with 4 μm in diameter and spacing, 18 μm in height, and 30° in tilting. The refractive index of the PEG pillars is ≈1.47, and we assume that reflected rays on the pillar surfaces do not affect the letter visibility. Figure 6d,e shows the results of ray-tracing simulation

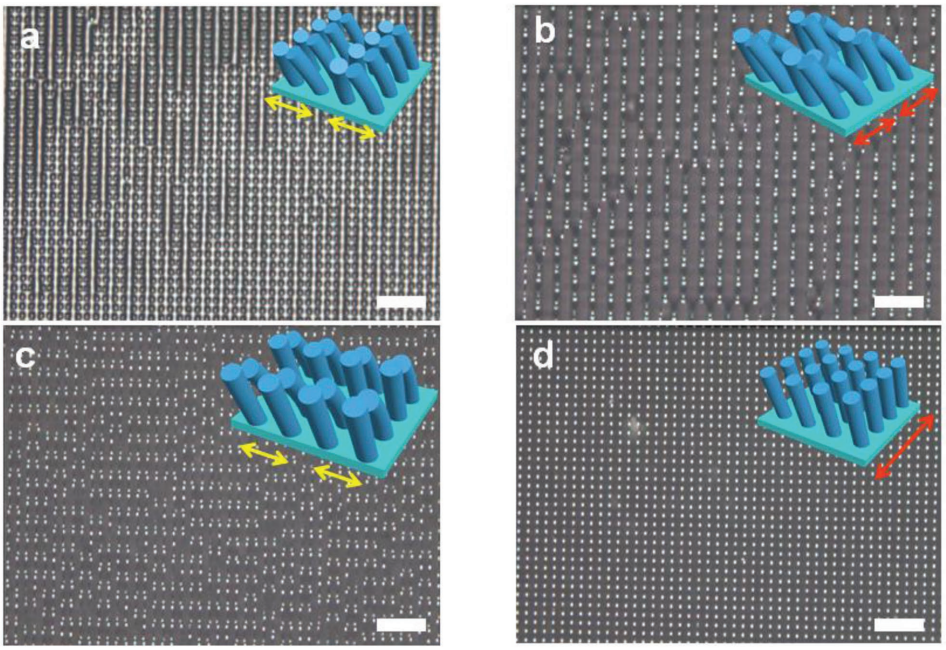

Figure 5. Optical images of sequential clustering and recovery of slanted pillars. a) Two pillars clustered in lateral direction (as indicated by yellow arrows in the inset) during water evaporation along the direction of the slanted pillars (as indicated by red arrows). b) Four pillars are clustered after evaporating water between the slanted pillars. c,d) After ≈ 1–2 min, pillars are recovered in the lateral direction because c) the displacement between pillars in the lateral direction is higher than the slanted direction, followed by d) recovery of the pillars in the slanted direction. The scale bars are 20 µm.

of the incident light through slanted pillars, while Figure 6f,g shows the simulation through clustered pillars. Few rays can transmit through the slanted pillars (Figure 6d), corresponding to the low intensity in slanted ones (Figure 6e). When the incident rays go through clustered pillars, the intensity becomes higher as shown in Figure 6g. Here, we assume the change of refractive index of hydrogel after swelling is trivial. The refractive index of the hydrogel after swelling (with 60% volume increase) is calculated as 1.42 when we regard the hydrogel as a simple mixture of PEG (83%, a refractive index of 1.47) and water (17%, a refractive index of 1.33).[22]

In summary, we have studied clustering and self-recovery of slanted hydrogel micropillars via in situ monitoring of these events using an optical microscope and an environmental scanning electron microscope, which can be attributed to the change of modulus during water drying from the internal network structure. When pillars are short (AR < 3), the hydrogel pillars do not cluster upon swelling because the capillary force is not enough to overcome the elastic restoring force. When pillars are tall (AR > 6), F_{res}/F_{adh} ratio is smaller than unity and the pillars are clustered and cannot be recovered. At AR = 3–6, F_{res}/F_{adh} ratio is larger than unity; pillars will recover to their original state. The sequential clustering and the recovery of slanted pillars are further explained by the difference of distance between in lateral and along the slanted direction. Furthermore, we show change of optical transparency by the clustering and recovery of the slanted micropillars. The study of mechanical deformation slanted hydrogel pillars and their recovery offers new insights into manipulation and actuation of micropillars in water environment. They will find potential applications, including directing cell alignment and cell and DNA sorting in microfluidic devices.

Experimental Section

Fabrication of the Si Masters: Slanted silicon pillar masters were fabricated on a p-type Si (100) wafer that were cut into a 10 × 10 mm^2 rectangle by photolithography, followed by slanted plasma etching. The Si substrate had a convex disk pattern with a 2 µm thick SiO_2 mask. The diameters of the holes were 2, 4, and 8 µm, respectively. The pitch of each pattern was double of the disk diameter. Therefore, the patterns were spaced 2, 4, and 8 µm apart from each other, respectively. Slanted plasma etching was performed using a Faraday cage in an inductively coupled plasma system.[18] The Faraday cage was fixed to the electrode. Because the cage formed a closed box, the electric potential was uniform and unaffected by outside electric fields. Therefore, the ion-incident angle (ϕ), defined as the angle between the direction of ion incidence and the surface normal to the substrate, could be controlled by varying the angle of the substrate holder. Slanted plasma etching was performed by a cyclic process consisting of alternating etching and deposition steps.[23] SF_6/Ar plasmas were used in the etching step while C_4F_8 plasmas were used in the deposition steps. The source power and bias voltage were 700 W and −50 V, respectively, in the etching step while 700 W and 0 V, respectively, in the deposition step. In the etching step, the flow rates of SF_6 and Ar were 30 and 5 sccm, respectively, and the chamber pressure was 10 mTorr. In the deposition step, the flow rate of C_4F_8 was 30 sccm, and the chamber pressure was 30 mTorr. The durations of etching and deposition steps were 40 and 12 s, respectively. After the pillars were formed, the samples were ashed at 500 °C for 1 h in order to remove the residual fluorocarbon films deposited on the pillars from the previous etching steps. The SiO_2 masks were removed by wet chemical etching in an aqueous HF solution for 4 min. The samples were subsequently rinsed with deionized water in an ultrasonicator (JAC-1505, KODO) for 5 min, and dried by nitrogen gas.

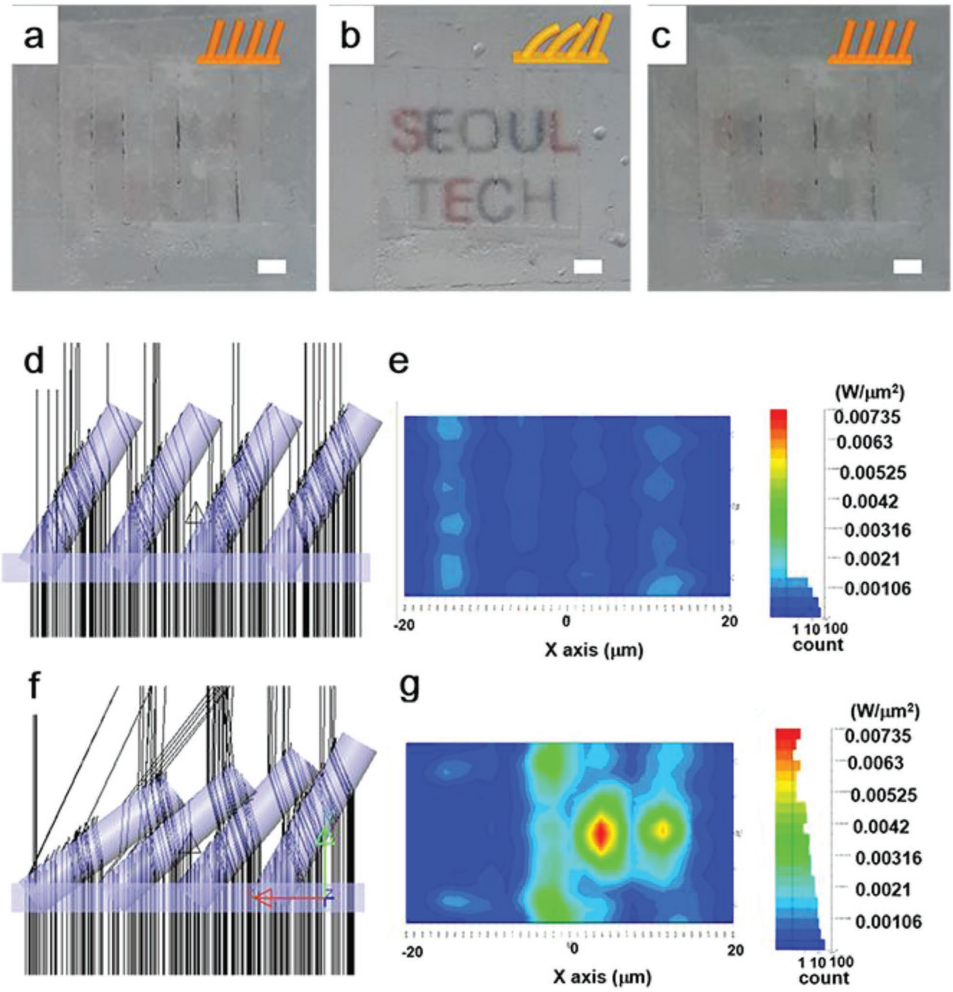

Figure 6. Optical microscopic images showing switching transparency of a film consisted of hydrogel pillars. a) Before swelling, b) after swelling, and c) after shape recovery. d) Ray tracing simulation of the incident light through slanted pillars. We removed rays reflected on the pillar surface because it does not affect the letter visibility. e) Light intensity obtained by the ray tracing. f) A ray-tracing simulation of incident light through clustered slanted pillars. g) Light intensity through the film of the clustered slanted pillars. The scale bars are 2 mm.

Preparation of PDMS Molds: PDMS (Sylgard 184, Dow Corning) prepolymers were mixed with curing agents in a weight ratio of 10:1. Then, they were poured onto the above fabricated Si master. After cross-linking at 60 °C for more than 4 h, the PDMS mold was peeled off from the master.

Fabrication of PEGDA Hydrogel Pillars: The PEGDA prepolymer was prepared by blending 99 wt% of PEGDA (average molecular weight M_n = 700, Sigma-Aldrich) with 1 wt% of 2-hydroxy-2-methylpropiophenone (Darocur 1173, Sigma-Aldrich). The mixture was placed onto the prepared PDMS mold and covered by a poly(ethylene terephthalate) (PET) film, followed by UV exposure for 90 s (FusionCure 360-08, 352 nm, 13 W). Subsequently, the PDMS mold was peeled off from the cross-linked PEGDA.

Examination of Clustering Events: The prepared PEGDA hydrogel pillar arrays (diameter D = 2, 4, 8, and 10 μm with the same spacing S, height H = 10, 12, and 18 μm, the tilt angle ϕ = 30°) were bonded onto a glass slide using a carbon tape. Then water was dropped on the samples and waited for more than 5 min to allow the hydrogel pillars to be fully swollen (see Figure S5 in the Supporting Information). After swelling the hydrogel micropillars, the excess water was removed by a porous paper for the observation of the clustering and recovery behaviors under an optical microscope (Olympus BX51M).

In Situ Imaging of Clustering and Recovery of Hydrogel Pillars: The dynamics of water condensation/evaporation were imaged using an FEI Quanta 200 field emission gun (FEG) ESEM at 30 kV voltage. In brief, the chamber was first vacuumed to 1 Torr and cooled to −12 °C by a Peltier element. After the temperature became stabilized, the water vapor pressure was gradually increased to ≈4.5 Torr to enable the continuous water condensation on the surface. During this step, the temperature of the Peltier element gradually increased to ≈ −2.2 °C due to the heat released during the condensation. To stop the condensation and evaporate the deposited water, the water vapor pressure was decreased to ≈3 Torr, and the stage was gradually heated to 0 °C in the meantime. During this process, a series of images were taken every 1 s to capture the recovery process of the pillars in situ.

Measurement of Elastic Modulus of Hydrogels by AFM: The elastic moduli of hydrogels in both swollen/dried state were measured utilizing the nanoindentation mode of multimode AFM (Nanowizard 3, JPK Instruments). Force modulation mode cantilevers (length = 225 mm, width = 27 mm, spring constant = 1.6 N m^{-1}) with pyramid shape tips and aluminum back coatings were used. About 230 force–distance curves were taken for each hydrogel sample in 10 mm × 10 mm area and then batch processed through JPK Data Processing software provided by the manufacturer. The elastic moduli were calculated from

each force spectroscopic curve with applying modified Sneddon fit for pyramid shape indentors with half-angle to a face degree of 19.47°, and a Poisson's ratio of 0.5. Calculated elastic modulus values were then statistically fitted to follow a normal distribution for each sample to take.

Supporting Information

Supporting Information is available from the Wiley Online Library or from the author.

Acknowledgements

H.L. and J.-H.K. contributed equally to this work. This work was supported by the National Research Foundation of Korea (NRF) grant funded by the Korea government (MEST) (2016R1A2B4013640 and 2018R1A2B6002410) and the Commercialization Promotion Agency for R&D Outcomes Grant funded by the Korean Government (MSIP) (2015, Joint Research Corporations Support Program). S.Y. acknowledges partial support by National Science Foundation (NSF) EFRI-ODISSEI grant (#EFRI 13–31583) and University Research Foundation grant from University of Pennsylvania.

Conflict of Interest

The authors declare no conflict of interest.

Keywords

capillary force, hydrogel, micropillar, modulus, transparency

Received: July 26, 2018
Revised: September 3, 2018
Published online: October 17, 2018

[1] A. K. Geim, S. V. Dubonos, I. V. Grigorieva, K. S. Novoselov, A. A. Zhukov, S. Y. Shapoval, *Nat. Mater.* **2003**, *2*, 461.
[2] M. Micciché, E. Arzt, E. Kroner, *ACS Appl. Mater. Interfaces* **2014**, *6*, 7076.
[3] S. Y. Lee, Y. Rahmawan, S. Yang, *ACS Appl. Mater. Interfaces* **2015**, *7*, 24197.
[4] E. Zanchetta, E. Guidi, G. Della Giustina, M. Sorgato, M. Krampera, G. Bassi, R. Di Liddo, G. Lucchetta, M. Teresa Conconi, G. Brusatin, *ACS Appl. Mater. Interfaces* **2015**, *7*, 7273.
[5] D. Copic, S. J. Park, S. Tawfick, M. F. De Volder, A. J. Hart, *Lab Chip* **2011**, *11*, 1831.
[6] K. J. Morton, G. Nieberg, S. Bai, S. Y. Chou, *Nanotechnology* **2008**, *19*, 345301.
[7] Y. Zhang, C. W. Lo, J. A. Taylor, S. Yang, *Langmuir* **2006**, *22*, 8595.
[8] S. H. Kang, B. Pokroy, L. Mahadevan, J. Aizenberg, *ACS Nano* **2010**, *4*, 6323.
[9] H. Duan, J. K. Yang, K. K. Berggren, *Small* **2011**, *7*, 2661.
[10] D. Chandra, S. Yang, *Langmuir* **2009**, *25*, 10430.
[11] H. Yoon, M. K. Kwak, S. M. Kim, S. H. Sung, J. Lim, H. S. Suh, K. Y. Suh, K. Char, *Small* **2011**, *7*, 3005.
[12] M. K. Kwak, H. E. Jeong, T. I. Kim, H. Yoon, K. Y. Suh, *Soft Matter* **2010**, *6*, 1849.
[13] S. Guo, J. Xu, M. Xie, W. Huang, E. Yuan, Y. Liu, L. Fan, S. Cheng, S. Liu, F. Wang, B. Yuan, W. Dong, X. Zhang, W. Huang, X. Zhou, *ACS Appl. Mater. Interfaces* **2016**, *8*, 15917.
[14] C. M. Chen, S. Yang, *Adv. Mater.* **2014**, *26*, 1283.
[15] S. M. Kim, J. Kim, S. M. Kang, S. Jang, D. Kang, S. E. Moon, H. N. Kim, H. Yoon, *Small* **2016**, *12*, 3764.
[16] M. Matsunaga, M. Aizenberg, J. Aizenberg, *J. Am. Chem. Soc.* **2011**, *133*, 5545.
[17] S. M. Kim, S. M. Kang, C. Lee, S. Jang, J. Kim, H. Seo, W. G. Bae, S. Yang, H. Yoon, *J. Mater. Chem. C* **2016**, *4*, 9608.
[18] D. H. Kang, S. M. Kim, B. Lee, H. Yoon, K. Y. Suh, *Analyst* **2013**, *138*, 6230.
[19] M. Guvendiren, S. Yang, J. A. Burdick, *Adv. Funct. Mater.* **2009**, *19*, 3038.
[20] C. Pang, T. I. Kim, W. G. Bae, D. Kang, S. M. Kim, K. Y. Suh, *Adv. Mater.* **2012**, *24*, 475.
[21] S.-W. Cho, C.-K. Kim, J.-K. Lee, S. H. Moon, H. Chae, *J. Vac. Sci. Technol., A* **2012**, *30*, 051301.
[22] J. Brandrup, E. H. Immergut, E. A. Grulke, *Polymer Handbook*, 4th ed., John Wiley & Sons, Inc., New York, NY **1999**.
[23] R. Digilov, *Langmuir* **2000**, *16*, 1424.

